Pairing effects on the collectivity of quadrupole states around ^{32}Mg

M. Yamagami[1] and Nguyen Van Giai[2]
[1]*Department of Physics, Graduate School of Science, Kyoto University, Kyoto 606-8502, Japan*
[2]*Institut de Physique Nucléaire, IN$_2$P$_3$-CNRS, 91406 Orsay Cedex, France*
(Received 11 July 2003; published 1 March 2004)

The first 2^+ states in $N=20$ isotones including neutron-rich nuclei ^{32}Mg and ^{30}Ne are studied by the Hartree-Fock-Bogoliubov plus quasiparticle random phase approximation method based on the Green's function approach. The residual interaction between the quasiparticles is consistently derived from the Hamiltonian density of Skyrme interactions with explicit velocity dependence. The $B(E2, 0_1^+ \rightarrow 2_1^+)$ transition probabilities and the excitation energies of the first 2^+ states are well described within a single framework. We conclude that pairing effects account largely for the anomalously large $B(E2)$ value and the very low excitation energy in ^{32}Mg.

DOI: 10.1103/PhysRevC.69.034301 PACS number(s): 21.60.Jz

I. INTRODUCTION

The pioneering observation in 1975 of the anomalous binding energy gain in very neutron rich Na isotopes revealed the breaking of the $N=20$ shell closure and the possibility of deformation [1]. The evidences of the breaking of $N=20$ shell closure in neutron-rich Mg and Ne isotopes are more clearly seen from the observations of $E2$ properties, the large $B(E2)$ value, and the low excitation energies of the first 2^+ states in ^{32}Mg and ^{30}Ne [2–6].

Several theoretical studies have been done to describe the anomalous binding energy and $E2$ properties in neutron-rich nuclei around $N=20$. Constrained Hartree-Fock (HF) calculations of Na isotopes [7] have been performed and ^{31}Na was suggested as deformed. Early studies made by Wildenthal *et al.* [8] and Chung showed that shell model calculations within the *sd* shell model space cannot explain the extra binding energies in this region. Subsequent shell model calculations [9–11] have demonstrated that the inclusion of the *fp* shell into the shell model active space is essential. The effects of the breaking of the $N=20$ shell closure are clearly shown in the description of the $B(E2)$ values and the excitation energies in ^{32}Mg and ^{30}Ne [12–15]. The neutron $2p$-$2h$ configurations across the $N=20$ shell imply deformation of these nuclei. However, in the framework of the mean-field approximation, such as Skyrme Hartree-Fock-Bogoliubov (HFB) calculations, the calculated ground states in ^{32}Mg and ^{30}Ne turn out to be spherical (see, e.g., Refs. [16,17]). One possible way to describe the (dynamical) deformation is to include correlations beyond the mean field. Generator coordinate method [18–20] and antisymmetrized molecular dynamics calculations [21] have been done in this direction.

Nevertheless, the experimental evidence of deformation in ^{32}Mg is not well established. The energy ratios of the first 4^+ and 2^+ states, $E(4^+)/E(2^+)$, are 3.0 in ^{24}Mg [22] and 3.2 in ^{34}Mg [23], and these values are very close to the rigid rotor limit of 3.3. On the other hand, the ratio is 2.6 in ^{32}Mg [23,24], and this value is in between the rigid rotor limit and the harmonic vibration limit 2.0. Moreover, the $B(E2)$ value (in single-particle units) is 15.0 ± 2.5 in ^{32}Mg [2]. This value is larger than in the other stable $N=20$ isotones but smaller than in other deformed Mg isotopes (21.0 ± 5.8 in ^{24}Mg [22] and 19.2 ± 3.8 in ^{34}Mg [25]).

Generally speaking, the neutron $2p$-$2h$ configurations can originate not only from deformation effects but also from neutron pairing correlations. In the ^{32}Mg nucleus these two effects may coexist and make the large $B(E2)$ value and the low excitation energy of the 2^+ state. In shell model studies it is not clear which effect is more essential to describe these anomalous properties.

The purpose of this paper is to emphasize how neutron pairing correlations play an essential role in the description of $E2$ properties in ^{32}Mg and ^{30}Ne. The existence of neutron pairing correlations means the breaking of the $N=20$ shell closure. As we will see, the appearance of neutron pairing correlations is related to a special mechanism in loosely bound systems. We study the first 2^+ states in $N=20$ isotones in the framework of self-consistent quasiparticle random phase approximation (QRPA) with Skyrme interactions [26]. The QRPA equations are solved in coordinate space by using the Green's function method [27]. To emphasize the role of neutron pairing correlations, spherical symmetry is imposed on our QRPA calculations. The residual interaction between the quasiparticles is self-consistently derived from the Hamiltonian density of Skyrme interaction that has an explicit velocity dependence. We will show that the $B(E2)$ values and the excitation energies of the first 2^+ states in $N=20$ isotones, from the stable nucleus ^{38}Ar to the neutron-rich nuclei ^{32}Mg and ^{30}Ne are well described within a single framework and a fixed parameter set. The paper is organized as follows. In Sec. II we briefly describe the HFB plus QRPA calculations that we have done. In Sec. III we present the general results for the ground states of the $N=20$ isotones studied here. In Sec. IV we discuss the calculated and experimental $E2$ properties of these nuclei. In Sec. V we show how self-consistent treatment of the residual interactions plays crucial role in describing very low lying states in ^{32}Mg and ^{30}Ne. Conclusions are drawn in Sec. VI.

II. HFB PLUS QRPA CALCULATIONS

A. Formulation

We use the approach of self-consistent HFB plus QRPA calculations with Skyrme interactions [26,27]. By self-

consistent we mean that the HFB mean fields are determined self-consistently from an effective force and the residual interaction of the QRPA problem is derived from the same force. The QRPA problem is solved by the response function method in coordinate space. A detailed account of the method can be found in Ref. [27]. Here, we just recall the main steps of the calculation. The QRPA Green's function **G** is solution of a Bethe-Salpeter equation,

$$\mathbf{G} = \mathbf{G}_0 + \mathbf{G}_0\mathbf{V}\mathbf{G}. \tag{1}$$

The knowledge of **G** allows one to construct the response function of the system to a general external field, and the strength distribution of the transition operator corresponding to the chosen field is just proportional to the imaginary part of the response function.

In Eq. (1) the unperturbed Green's function $\mathbf{G}_0$ is defined as

$$G_0^{\alpha\beta}(\boldsymbol{r}\sigma,\boldsymbol{r}'\sigma';\omega) = \sum_{i,j} \frac{W_{i,j}^{\alpha 1}(\boldsymbol{r}\sigma)[W_{i,j}^{\beta 1*}(\boldsymbol{r}'\sigma')]_-}{\hbar\omega - (E_i + E_j) + i\eta} - \frac{W_{i,j}^{\alpha 2*}(\boldsymbol{r}\sigma)[W_{i,j}^{\beta 2}(\boldsymbol{r}'\sigma')]_-}{\hbar\omega + (E_i + E_j) + i\eta}, \tag{2}$$

where the functions $W(\boldsymbol{r}\sigma)$ are introduced as

$$W_{i,j}(\boldsymbol{r}\sigma) = \begin{pmatrix} U_i(\boldsymbol{r}\sigma)V_j(\boldsymbol{r}\sigma) & V_i(\boldsymbol{r},\sigma)U_j(\boldsymbol{r}\sigma) \\ U_i(\boldsymbol{r}\sigma)U_j(\boldsymbol{r}\overline{\sigma}) & V_i(\boldsymbol{r}\sigma)V_j(\boldsymbol{r}\overline{\sigma}) \\ -V_i(\boldsymbol{r}\sigma)V_j(\boldsymbol{r}\overline{\sigma}) & -U_i(\boldsymbol{r}\sigma)U_j(\boldsymbol{r}\overline{\sigma}) \end{pmatrix}. \tag{3}$$

Here, the $U(\boldsymbol{r}), V(\boldsymbol{r})$ are quasiparticle wave functions, the index $\alpha(\alpha=1,2,3)$ stands for particle-hole (*ph*), particle-particle (*pp*), and hole-hole (*hh*) channels. The notation $f(\boldsymbol{r}\overline{\sigma}) \equiv -2\sigma f(\boldsymbol{r}-\sigma)$ indicates time reversal and $[W_{i,j}]_- \equiv W_{i,j} - W_{j,i}$.

The residual interaction **V** between quasiparticles is derived from the Hamiltonian density $\langle H\rangle$ of Skyrme interaction by the so-called Landau procedure,

$$V_{\alpha\beta}(\boldsymbol{r}\sigma\tau,\boldsymbol{r}'\sigma'\tau') = \frac{\partial^2\langle H\rangle}{\partial\rho_\beta(\boldsymbol{r}'\sigma'\tau')\,\partial\rho_{\overline{\alpha}}(\boldsymbol{r}\sigma\tau)}. \tag{4}$$

The notation $\overline{\alpha}$ means that whenever α is *pp* (*hh*) then $\overline{\alpha}$ is *hh* (*pp*). The normal and abnormal densities are defined as

$$\begin{pmatrix} \rho_{ph}(\boldsymbol{r}\sigma) \\ \rho_{pp}(\boldsymbol{r}\sigma) \\ \rho_{hh}(\boldsymbol{r}\sigma) \end{pmatrix} = \begin{pmatrix} \rho(\boldsymbol{r}\sigma) \\ \kappa(\boldsymbol{r}\sigma) \\ \overline{\kappa}(\boldsymbol{r}\sigma) \end{pmatrix} = \begin{pmatrix} \langle 0|\psi^\dagger(\boldsymbol{r}\sigma)\psi(\boldsymbol{r}\sigma)|0\rangle \\ \langle 0|\psi(\boldsymbol{r}\overline{\sigma})\psi(\boldsymbol{r}\sigma)|0\rangle \\ \langle 0|\psi^\dagger(\boldsymbol{r}\sigma)\psi^\dagger(\boldsymbol{r}\overline{\sigma})|0\rangle \end{pmatrix}. \tag{5}$$

The (*ph*,*ph*) channel of the residual interaction has an explicit momentum dependence,

$$V_{ph,ph}(\boldsymbol{r}\sigma\tau,\boldsymbol{r}'\sigma'\tau') = \{a + b(\overleftarrow{\Delta}_U + \overleftarrow{\Delta}_V + \vec{\Delta}_U + \vec{\Delta}_V) + b(\overleftarrow{\nabla}_U - \overleftarrow{\nabla}_V)\cdot(\vec{\nabla}_U - \vec{\nabla}_V) + c(\overleftarrow{\nabla}_U + \overleftarrow{\nabla}_V)\cdot(\vec{\nabla}_U + \vec{\nabla}_V)\}\delta(\boldsymbol{r}-\boldsymbol{r}'), \tag{6}$$

where the coefficients *a*, *b*, and *c* are functions of Skyrme parameters [28,29]. The operators with $\leftarrow(\rightarrow)$ act on the coordinate $\boldsymbol{r}(\boldsymbol{r}')$, and the operators with the index $U(V)$ operate on the quasiparticle wave functions $U(\boldsymbol{r})$ $[V(\boldsymbol{r})]$ only. In the previous study [27], the Landau-Migdal limit of the (*ph*,*ph*) residual interaction, where the interacting particle and hole have the Fermi momentum and the transferred momentum is zero [30], was used to reduce the numerical task, but the full momentum dependence is now explicitly treated in the present calculations. The spin-spin parts of the residual interaction are dropped, because we calculate only natural parity (non-spin-flip) excitations. The Coulomb and spin-orbit residual interactions are also dropped.

In a fully consistent calculation the spurious center-of-mass state should come out at zero energy. But, in practice, several approximations are imposed on the self-consistent residual interaction, Eq. (6), to reduce the computational efforts. Then, the self-consistency between the mean field and the residual interaction is broken. To recover the self-consistency approximately, the residual interaction has to be renormalized, $\mathbf{V}\rightarrow f_R\mathbf{V}$, so as to have the spurious state at zero energy. Here, f_R is a renormalization factor. In $N=20$ isotones, for example, $f_R\approx 0.93$ is used for calculations with self-consistent residual interaction Eq. (6). About 7% deviation from unity is coming from the approximation that we drop the spin-spin, spin-orbit, and Coulomb parts of the residual interaction. If the terms depending on ∇ operator are neglected, $f_R\approx 0.76$. If the Landau-Migdal force is used, $f_R \approx 0.60$.

In Sec. V, we discuss how the self-consistency of the residual interaction plays a crucial role in obtaining QRPA low-lying solutions close to the critical energy.

B. Inputs

We apply the above formalism to study the first 2^+ states in $N=20$ isotones, ^{30}Ne, ^{32}Mg, ^{34}Si, ^{36}S, and ^{38}Ar. The ground states are given by Skyrme-HFB calculations. The HFB equation is diagonalized on a Skyrme-HF basis calculated in coordinate space with a box boundary condition [31–33]. The box radius is 20 fm. Spherical symmetry is imposed on quasiparticle wave functions. The quasiparticle cutoff energy is taken to be $E_{cut}=50$ MeV, and the angular momentum cutoff is $l_{max}=7\hbar$ in our HFB and QRPA calculations.

The Skyrme parameters SkM*[34] and SkP[35] are used for the HF mean field, and the density-dependent, zero-range pairing interaction

$$V_{pair}(\boldsymbol{r},\boldsymbol{r}') = V_{pair}\left[1 - \left(\frac{\rho(\boldsymbol{r})}{\rho_c}\right)^\alpha\right]\delta(\boldsymbol{r}-\boldsymbol{r}') \tag{7}$$

is adopted for the pairing field. The parameters α and ρ_c are fixed as $\alpha=1$ and $\rho_c=0.16$ fm^{-3}. The strength V_{pair} is determined so as to reproduce the experimental neutron pairing gap in ^{30}Ne, $\Delta_{n,expt.}(^{30}\text{Ne})=1.26$ MeV. ^{30}Ne is the lightest mass even-even $N=20$ nucleus. The experimental pairing gaps are extracted by using the three-point mass difference formula [38], $\Delta_n(N) \equiv \Delta_n^{(3)}(N-1) = [(-1)^N/2][E(N-2) + E(N) - 2E(N-1)]$. On the other hand, the average pairing gap in HFB calculations is defined as the integral of the

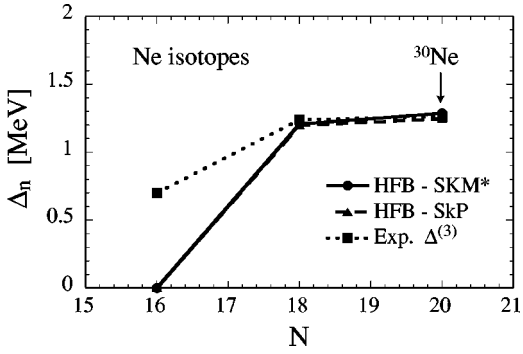

FIG. 1. HFB neutron pairing gaps in ^{26,28,30}Ne calculated with SkM* and SkP. The pairing strengths V_{pair} are fixed so as to reproduce the experimental neutron gap in ^{30}Ne. The experimental pairing gaps are extracted by using the three-point mass difference formula [38].

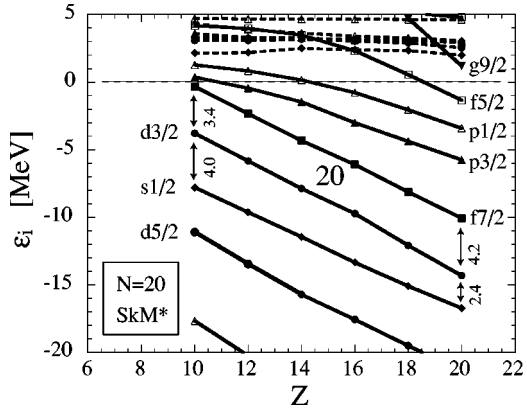

FIG. 2. HF neutron single-particle levels in $N=20$ isotones calculated with SkM*. Solid lines correspond to bound and resonance-like states, dashed lines to positive energy discretized states.

pairing field, $\overline{\Delta}_n = \int d\vec{r}\tilde{\rho}_n(\vec{r})\Delta_n(\vec{r}) / \int d\vec{r}\tilde{\rho}_n(\vec{r})$ [39]. The pairing strength adopted for SkM* is $V_{pair} = -418$ MeV fm^{-3}, and for SkP, $V_{pair} = -400$ MeV fm^{-3}. Figure 1 shows the experimental and the calculated pairing gaps in ^{26,28,30}Ne. With these Skyrme parameters and pairing strengths, we get finite pairing gap in ^{30}Ne (vanishing of $N=20$ shell gap) and zero pairing gap in ^{26}Ne (appearance of $N=16$ shell gap) at the same time.

III. GROUND STATE PROPERTIES

Figure 2 shows the neutron single-particle levels in $N=20$ isotones calculated in HF with SkM*. Results with SkP are qualitatively the same. The $N=16$ shell gaps change from 2.4 MeV in ^{40}Ca to 4.0 MeV in ^{30}Ne. Within HF we can describe the appearance of $N=16$ magic number. On the other hand, the $N=20$ shell gaps change slowly from 4.2 MeV in ^{40}Ca to 3.4 MeV in ^{30}Ne, because $2d_{3/2}$ and $1f_{7/2}$ orbits do not vary much around zero energy due to the large centrifugal barriers [40]. It seems difficult to explain the breaking of the $N=20$ shell closure within HF.

An important feature in Fig. 2 is the behavior of low-l orbits, $2p_{3/2}$ and $2p_{1/2}$, in the fp shell. As the proton number decreases, the single-particle energies of the high-l orbit $1f_{7/2}$ change almost linearly while the changes of $2p_{3/2}$ and $2p_{1/2}$ energies become very slow around zero energy. Moreover, the spin-orbit splitting of $2p_{3/2}$ and $2p_{1/2}$ states becomes smaller. As pointed out by Hamamoto *et al.* [40], these effects can be understood by different l dependences of the kinetic energy and the spin-orbit form factor as the single-particle energy comes close to zero, originating from the difference of the height of the centrifugal barriers. Because of these different l dependences of the single-particle energies, the level density in the fp shell becomes higher with decreasing proton number, and the three orbits $1f_{7/2}$, $2p_{3/2}$, and $2p_{1/2}$ become almost degenerate in ^{30}Ne. We can describe this behavior naturally by solving the HF and HFB equations in coordinate space but it is difficult to get this property by the methods based on the harmonic oscillator basis.

Figure 3 shows the HFB neutron and proton pairing gaps in $N=20$ isotones calculated with SkM* and SkP. The pairing strengths are adjusted so as to reproduce the experimental neutron pairing gap in ^{30}Ne. As the proton number increases, the neutron pairing gaps decrease monotonically and eventually, the neutron pairing gap becomes zero (for both SkM* and SkP) in ^{38}Ar as expected in stable $N=20$ nuclei. The interesting point is that the $N=20$ shell gap itself changes very moderately but the calculated neutron pairing gap changes considerably from 1.26 MeV in ^{30}Ne to zero in ^{38}Ar. The mechanism can be understood by the increase of the level density in the fp shell when the proton number decreases, as noted above. Within HFB calculations with spherical symmetry, the $N=20$ shell gap is naturally broken by neutron pairing correlations. Since the neutron pairing gap is adjusted in ^{30}Ne it remains close in ^{32}Mg for both Skyrme parameters, but large differences are seen in ^{34}Si and ^{36}S. On the other hand, the calculated proton pairing gaps with both Skyrme parameters are quantitatively similar.

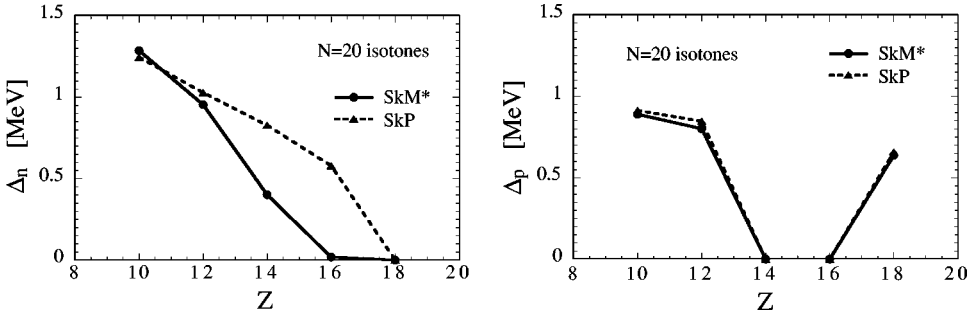

FIG. 3. The neutron and proton pairing gaps in $N=20$ isotones calculated in HFB with SkM* and SkP.

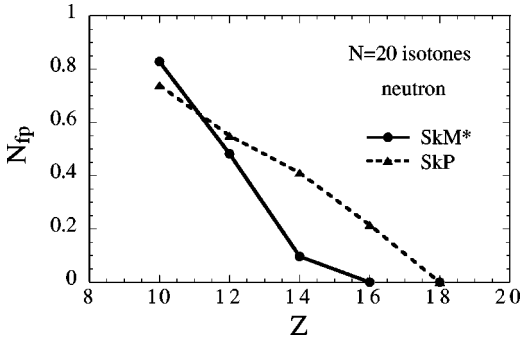

FIG. 4. Average number of neutrons in the fp shell in $N=20$ isotones calculated in HFB with SkM* and SkP.

Figure 4 shows the average number of neutrons N_{fp} in the fp shell in $N=20$ isotones, calculated in HFB with SkM* and SkP. According to the change of the neutron pairing gaps, N_{fp} decreases monotonically from $\simeq 0.8$ in ^{30}Ne to $\simeq 0.5$ in ^{32}Mg. These values are very different from the prediction of the "island of inversion," $N_{fp}=2$ [11] and Monte Carlo shell model, $N_{fp} \geqslant 2$ in ^{30}Ne and ^{32}Mg [14].

Because Skyrme parameters are usually adjusted by using properties of selected β-stable nuclei, the $N=20$ shell gaps in neutron-rich nuclei calculated with various Skyrme parameters have large discrepancies. The shell gap in ^{30}Ne is 3.4 MeV in SkM* and 3.7 MeV in SkP. On the other hand, the modern version of Skyrme parameters, for example, SLy4 [36] and SkI4 [37] that are considered to have better isospin properties, give very large shell gaps, 5.2 MeV and 6.9 MeV, respectively. The description of the ground state properties such as neutron pairing correlations, and the low-lying collective states are very sensitive to the shell structure. We found that SkM* and SkP having smaller $N=20$ shell gap can reproduce not only the ground state properties shown above, but also, as seen in the following section, the $E2$ properties in $N=20$ isotones very well within a single parameter set consistently. On the other hand, it is difficult to describe the breaking of the $N=20$ shell closure with SLy4 and SkI4. The Skyrme parameter dependence of the shell structure in $N=20$ isotones is extensively studied in Ref. [17].

In the framework of the mean-field approximation, irrespective of relativistic or nonrelativistic approaches, the ground states of ^{30}Ne and ^{32}Mg have been found to be spherical (see, for example, Refs. [16–20,41–45]). Reinhard *et al.* [17] have made systematic studies of quadrupole deformation around $N=20$ neutron-rich nuclei by Skyrme-HF plus BCS pairing approach with ten kinds of Skyrme parametrizations and different pairing treatments, surface-type and volume-type pairing. They found that all Skyrme parametrizations give spherical ground state in ^{30}Ne and ^{32}Mg irrespective of treatments of pairing correlations. Terasaki *et al.* [16] have studied quadrupole deformations of Mg isotopes by means of Skyrme-HFB calculations. They also found a spherical ground state in ^{32}Mg.

In our spherical Skyrme-HFB calculations, we used a large cutoff energy of 50 MeV, and the pairing strength is adjusted in ^{30}Ne. On the other hand, in deformed Skyrme-HF plus BCS or Skyrme-HFB calculations, small cutoff energies, typically 5 MeV, are used and the pairing strengths are adjusted in different mass regions. Therefore, it is not clear that the ground states in ^{30}Ne and ^{32}Mg are spherical in calculations with the same inputs as ours. The existence of spherical solutions is clear, because we get QRPA solutions as shown in the following section. In principle, we cannot exclude the possibility that the prolate states become the ground states. However, we expect that the ground states are spherical because all mean-field calculations that have been already performed give spherical ground states, irrespective of relativistic or nonrelativistic approaches with various types of effective interactions, as noted above.

IV. $B(E2)$ VALUES AND EXCITATION ENERGIES

We have calculated the first 2^+ states in $N=20$ isotones in HFB plus QRPA with Skyrme interactions, assuming spherical symmetry. Our aim is to investigate whether these 2^+ states can be described as vibrational states built on the spherical ground states.

In Fig. 5 our results of QRPA calculations with SkM* are compared with the results of the Monte Carlo shell model (MCSM) [14], and the available experimental data [2,3,6,22]. Our QRPA results are in good agreement with the experimental data and they are consistent with the MCSM prediction of the $B(E2)$ value in ^{30}Ne. The latter case has been measured very recently, but the error bar is still large [6]. The QRPA calculations have been done with SkM* and

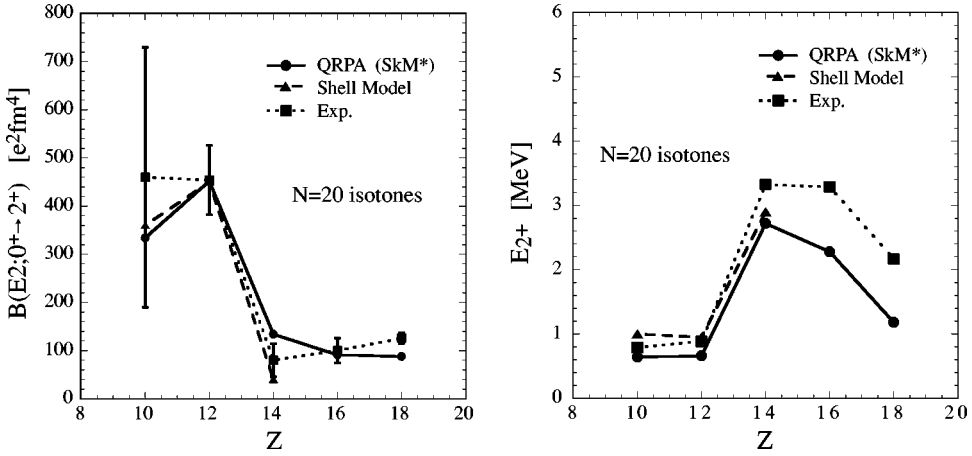

FIG. 5. The $B(E2, 0_1^+ \rightarrow 2_1^+)$ transition probabilities and excitation energies of the first 2^+ states in $N=20$ isotones calculated in QRPA with SkM*. For comparison the calculations of MCSM [14] and the available experimental data [2,3,6,22] are shown.

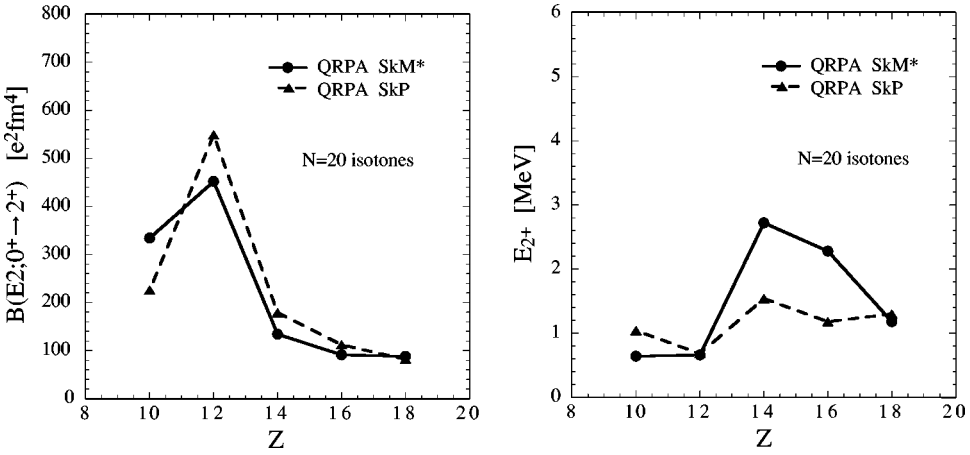

FIG. 6. The $B(E2, 0_1^+ \rightarrow 2_1^+)$ transition probabilities and excitation energies of the first 2^+ states calculated in QRPA with SkM* and SkP.

the fixed pairing strength $V_0 = -418$ MeV fm^{-3}, the choice of which is explained in Sec. II B. The general properties of the first 2^+ states in $N=20$ isotones, namely, very large $B(E2)$ values and very low excitation energies in ^{32}Mg and ^{30}Ne are well reproduced within a single framework.

To check the interaction dependence we have carried out QRPA calculations with SkP. Figure 6 shows the $B(E2)$ values and excitation energies of the first 2^+ states with SkM* and SkP. Concerning the $B(E2)$ values we get similar results, especially very large $B(E2)$ values in ^{32}Mg and ^{30}Ne. On the other hand, large differences are seen in the excitation energies in ^{34}Si and ^{36}S. This can be understood by the difference in the neutron pairing correlations shown in Fig. 3. In ^{30}Ne, ^{32}Mg, and ^{38}Ar the neutron pairing gaps calculated with SkM* and SkP are almost the same while they are somewhat different in ^{34}Si and ^{36}S. Because the neutron pairing gaps are larger in SkP than in SkM*, the excitation energies become lower with SkP than with SkM*.

We now explain how the neutron pairing correlations are important to make the $B(E2)$ values larger and the excitation energies lower. To see which two-quasiparticle configurations contribute to make the low-lying 2^+ states, we show the unperturbed isoscalar quadrupole strength functions in $N=20$ isotones calculated with SkM* in Fig. 7. The peaks indicated by solid (dotted) arrows correspond to proton (neutron) two-quasiparticle configurations. All these neutron two-quasiparticle configurations appear because of the neutron pairing correlations. Many peaks of the neutron configurations are seen in ^{30}Ne, ^{32}Mg. On the other hand, the neutron configurations are negligible in ^{34}Si and they completely disappear in ^{36}S. The $B(E2)$ values are primarily made of the proton configurations in the *sd* shell but the neutron configurations assist to make the $B(E2)$ values larger by coherence between protons and neutrons. Actually, if the neutron pairing correlations are neglected the $B(E2)$ values become very small and the excitation energies are sizably higher in ^{32}Mg and ^{30}Ne, as shown in Fig. 8. Under these considerations, we can conclude that the very large $B(E2)$ values and the very low excitation energies in ^{32}Mg and ^{30}Ne appear thanks to the presence of the neutron pairing correlations. We have seen in Sec. III that, around the drip line the origin of neutron pairing correlations lies in the different behavior of the

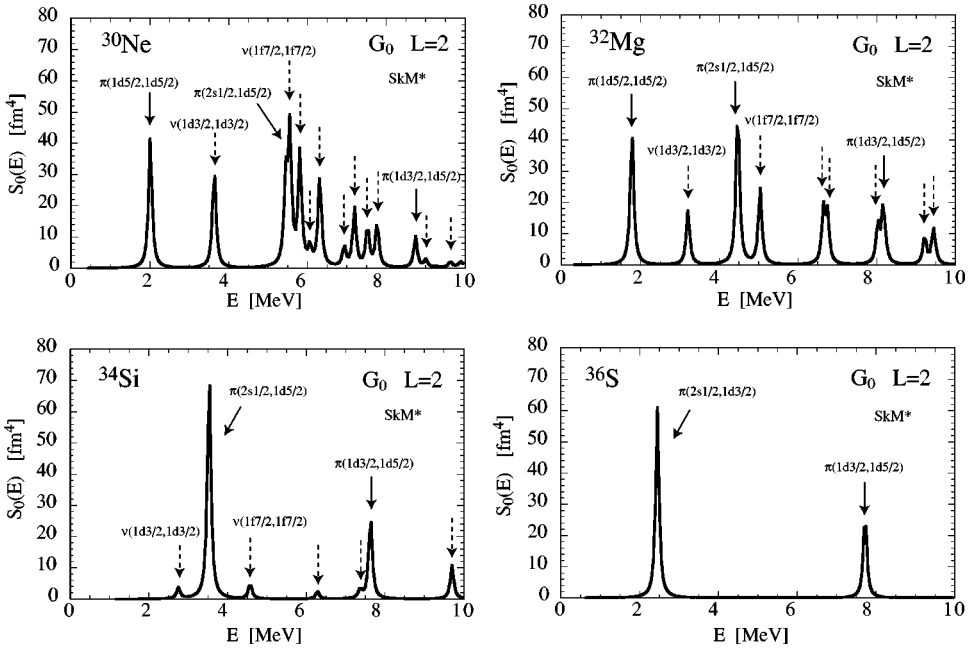

FIG. 7. The unperturbed isoscalar quadrupole strength functions in $N=20$ isotones calculated with SkM*. The peaks indicated by solid (dotted) arrows correspond to proton (neutron) two-quasiparticle configurations.

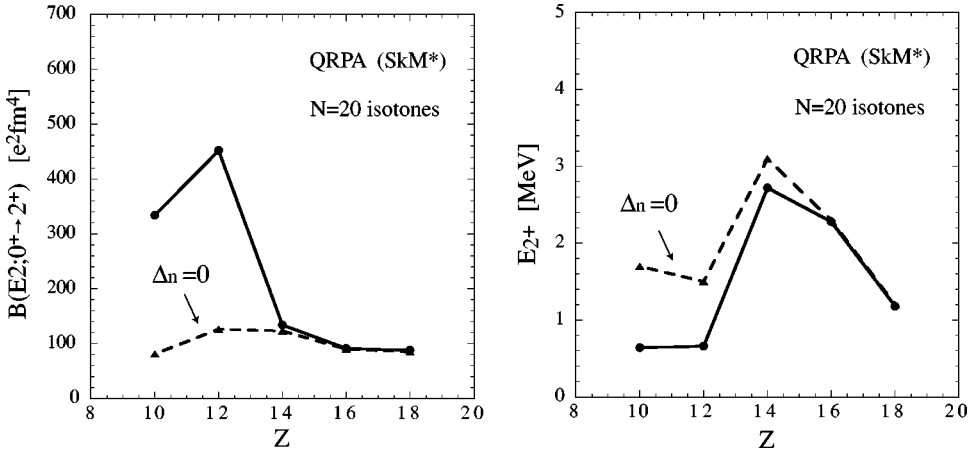

FIG. 8. The $B(E2,0_1^+\rightarrow 2_1^+)$ values and the excitation energies of the first 2^+ states in $N=20$ isotones calculated with/without neutron pairing correlations. Proton pairing is included in both cases.

single-particle levels with different orbital angular momentum l as the levels approach the separation threshold.

Generally speaking, neutron $2p$-$2h$ configurations across $N=20$ can originate from deformation effects or pairing effects. Both effects can *a priori* contribute in the nucleus ^{32}Mg. We have shown that a spherical QRPA description, i.e., putting emphasis on the pairing aspects and neglecting the possible deformation effects, can give very satisfactory results. In the previous studies based on shell model calculations [12–14] the importance of neutron $2p$-$2h$ configurations for describing the $B(E2)$ values in ^{32}Mg, ^{30}Ne was shown, but the respective roles of pairing and deformation were not clear.

V. STABILITY OF LOW-LYING QRPA SOLUTIONS

As is well known, when a QRPA eigenvalue is approaching zero the solution suffers instability and the transition probability diverges. Since our QRPA solutions for ^{32}Mg and ^{30}Ne have very low energies, we have to check whether the calculated $B(E2)$ values are really meaningful or just spurious results. Figure 9 shows the dependence of the $B(E2)$ value, excitation energy, and average neutron pairing gap on the pairing strength V_{pair} in ^{32}Mg. Here, the cutoff energy is fixed at $E_{cut}=50$ MeV. The solid line is calculated with the self-consistent residual interaction Eq. (6), the dotted line with a Landau-Migdal force without explicit velocity dependence, while the dashed line is obtained with a residual interaction where the terms in ∇ have been dropped.

If $|V_{pair}|$ increases, the excitation energy decreases and the $B(E2)$ value increases. This behavior is the result of two competing effects. First, the pairing gap and also the quasiparticle energies increase with increasing $|V_{pair}|$. Therefore, the two-quasiparticle energies and the QRPA excitation energies should increase and the $B(E2)$ values should decrease. Second, if $|V_{pair}|$ increases, many two-quasiparticle configurations can contribute to the 2^+ state and the collectivity increases. In this case the QRPA excitation energies would decrease and the $B(E2)$ values would increase. In the ^{32}Mg case the second effect wins (cf. Fig. 9). In the calculation with the self-consistent residual interaction, as $|V_{pair}|$ is increasing, the excitation energy becomes lower and the $B(E2)$ value increases linearly up to $|V_{pair}|\simeq 422$ MeV fm^{-3}. Above $|V_{pair}|\simeq 426$ MeV fm^{-3} the $B(E2)$ value starts to diverge. Because our adopted pairing strength is $V_{pair}=-418$ MeV fm^{-3}, we confirm that our QRPA solution is meaningful.

If simplified residual interactions are used (see the dashed and dotted curves of Fig. 9), the low-lying solutions are already collapsed at $|V_{pair}|=418$ MeV fm^{-3}. These calculations clearly show that a self-consistent treatment of the residual interaction plays a crucial role in describing these very low lying states.

On the other hand, if the solution is far enough from the

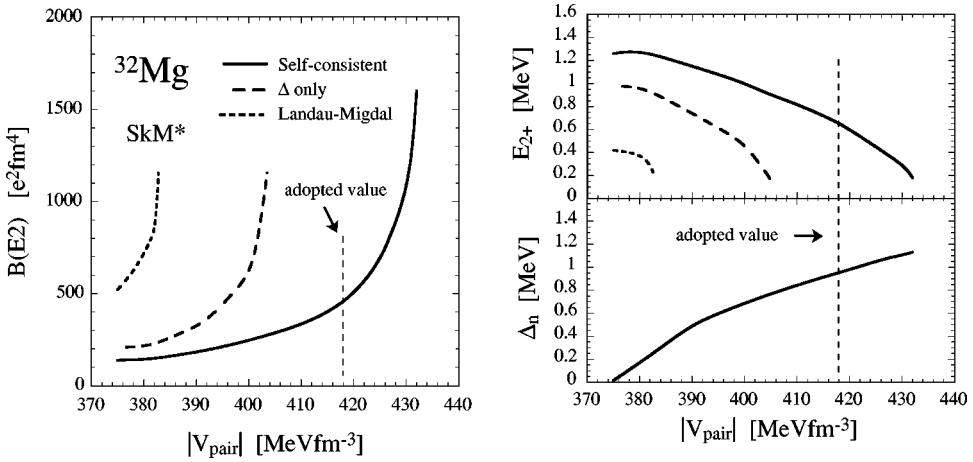

FIG. 9. The $B(E2)$ value and excitation energy of the first 2^+ state in ^{32}Mg calculated in QRPA with SkM*, as a function of the pairing strength V_{pair}. Three types of approximations for the residual interaction are examined: the solid line is a calculation with the self-consistent residual interaction, Eq. (6); the dashed line is obtained with a residual interaction where terms in ∇ are dropped; the dotted line corresponds to the Landau-Migdal force.

critical energy like in ^{34}Si, ^{36}S, and ^{38}Ar, the calculations with the self-consistent and the approximated residual interactions give stable solutions. In ^{34}Si, for instance, the $B(E2)$ value decreases by about 16% and the excitation energy increases by about 0.2 MeV at the adopted pairing strength when going from the self-consistent residual interaction to the Landau-Migdal force.

Another example can be found with the residual interaction dependence of $E2$ properties in oxygen isotopes [46]. The $B(E2)$ value in ^{20}O calculated with the self-consistent residual interaction is 34.1 e^2 fm^4. On the other hand, the $B(E2)$ value calculated with a Landau-Migdal force is 20.9 e^2 fm^4. In this case, the $B(E2)$ value increases by 64%. Thus, the self-consistent treatment of the residual interaction is always important for describing the low-lying states and for quantitative comparisons with experimental data, and it plays a crucial role qualitatively to describe very low-lying states like in ^{32}Mg and ^{30}Ne.

VI. CONCLUSION

We have studied the first 2^+ states in $N=20$ isotones by the HFB plus QRPA model with Skyrme interactions. The residual interaction is consistently derived from the Skyrme Hamiltonian, keeping all its explicit momentum dependence.

Because of the different behaviors of the neutron $1f_{7/2}$, $2p_{3/2}$, and $2p_{1/2}$ levels when the single-particle energies are approaching zero, the neutron pairing gaps have finite values. This mechanism breaks the $N=20$ magicity in ^{32}Mg and ^{30}Ne.

Within our consistent QRPA calculation with spherical symmetry the $B(E2)$ values and the excitation energies of the first 2^+ states in $N=20$ isotones including neutron-rich ^{32}Mg and ^{30}Ne are well described. The existing experimental data are reproduced quantitatively. The important role of the neutron pairing correlations is emphasized. If the neutron pairing is dropped, we cannot get the correct $B(E2)$ value and excitation energy in ^{32}Mg and ^{30}Ne. In the real ^{32}Mg nucleus, both neutron pairing and deformation effects may coexist and help to make the large $B(E2)$ value, but our calculation shows that neutron pairing correlations are essential.

ACKNOWLEDGMENTS

We acknowledge Professor K. Matsuyanagi for valuable discussions. We thank Professor T. Suzuki (Fukui) and Professor I. Hamamoto for useful comments. We also thank Dr. E. Khan for many discussions. One of the authors (M.Y.) is very grateful to the members of the Theory Group of IPN-Orsay for their hospitality during his stay. Numerical computation in this work was carried out at the Yukawa Institute Computer Facility.

[1] C. Thibault, R. Klapisch, C. Rigaud, A. M. Poskanzer, R. Prieels, L. Lessard, and W. Reisdorf, Phys. Rev. C **12**, 644 (1975).
[2] T. Motobayashi, Y. Ikeda, Y. Ando, K. Ieki, M. Inoue, N. Iwasa, T. Kikuchi, M. Kurokawa, S. Moriya, S. Ogawa, H. Murakami, S. Shimoura, Y. Yanagisawa, T. Nakamura, Y. Watanabe, M. Ishihara, T. Teranishi, H. Okuno, and R. F. Casten, Phys. Lett. B **346**, 9 (1995).
[3] D. Guillemaud-Mueller, C. Detraz, M. Langevin, F. Naulin, M. De Saint-Simon, C. Thibault, F. Touchard, and M. Epherre, Nucl. Phys. **A426**, 37 (1984).
[4] B. V. Pritychenko, T. Glasmacher, P. D. Cottle, M. Fauerbach, R. W. Ibbotson, K. W. Kemper, V. Maddalena, A. Navin, R. Ronningen, A. Sakharuk, H. Scheit, and V. G. Zelevinsky, Phys. Lett. B **461**, 322 (1999); **467**, 309(E) (1999).
[5] V. Chiste, A. Gillibert, A. Lepine-Szily, N. Alamanos, F. Auger, J. Barrette, F. Braga, M. D. Cortina-Gil, Z. Dlouhy, V. Lapoux, M. Lewitowicz, R. Lichtenthaler, R. Liguori Neto, S. M. Lukyanov, M. MacCormick, F. Marie, W. Mittig, F. de Oliveira Santos, N. A. Orr, A. N. Ostrowski, S. Ottini, A. Pakou, Yu. E. Penionzhkevich, P. Roussel-Chomaz, and J. L. Sida, Phys. Lett. B **514**, 233 (2001).
[6] Y. Yanagisawa, M. Notani, H. Sakurai, M. Kunibu, H. Akiyoshi, N. Aoi, H. Baba, K. Demichi, N. Fukuda, H. Hasegawa, Y. Higurashi, M. Ishihara, N. Iwasa, H. Iwasaki, T. Gomi, S. Kanno, M. Kurokawa, Y. U. Matsuyama, S. Michimasa, T. Minemura, T. Mizoi, T. Nakamura, A. Saito, M. Serata, S. Shimoura, T. Sugimoto, E. Takeshita, S. Takeuchi, K. Ue, K. Yamada, K. Yoneda, and T. Motobayashi, Phys. Lett. B **566**, 84 (2003).
[7] X. Campi, H. Flocard, A. K. Kerman, and S. Koonin, Nucl. Phys. **A251**, 193 (1975).
[8] B. H. Wildenthal and W. Chung, Phys. Rev. C **22**, 2260 (1980).
[9] A. Watt, R. P. Singhal, M. H. Storm, and R. R. Whitehead, J. Phys. G **7**, L145 (1981).
[10] A. Poves and J. Retamosa, Phys. Lett. B **184**, 311 (1987).
[11] E. K. Warburton, J. A. Becker, and B. A. Brown, Phys. Rev. C **41**, 1147 (1990).
[12] N. Fukunishi, T. Otsuka, and T. Sebe, Phys. Lett. B **296**, 279 (1992).
[13] E. Caurier, F. Nowacki, A. Poves, and J. Retamosa, Phys. Rev. C **58**, 2033 (1998).
[14] Y. Utsuno, T. Otsuka, T. Mizusaki, and M. Honma, Phys. Rev. C **60**, 054315 (1999).
[15] E. Caurier, F. Nowacki, and A. Poves, Nucl. Phys. **A693**, 374 (2001).
[16] J. Terasaki, H. Flocard, P.-H. Heenen, and P. Bonche, Nucl. Phys. **A621**, 706 (1997).
[17] P.-G. Reinhard, D. J. Dean, W. Nazarewicz, J. Dobaczewski, J. A. Maruhn, and M. R. Strayer, Phys. Rev. C **60**, 014316 (1999).
[18] S. Péru, M. Girod, and J. F. Berger, Eur. Phys. J. A **9**, 35 (2000).
[19] R. Rodriguez-Guzman, J. L. Egido, and L. M. Robledo, Nucl. Phys. **A709**, 201 (2002).
[20] R. Rodriguez-Guzman, J. L. Egido, and L. M. Robledo, Eur. Phys. J. A **17**, 37 (2003).

[21] M. Kimura and H. Horiuchi, Prog. Theor. Phys. **107**, 33 (2002).
[22] S. Raman, C. H. Malarkey, W. T. Milner, C. W. Nestor, Jr., and P. H. Stelson, At. Data Nucl. Data Tables **36**, 1 (1987).
[23] K. Yoneda, H. Sakurai, T. Gomi, T. Motobayashi, N. Aoi, N. Fukuda, U. Futakami, Z. Gacsi, Y. Higurashi, N. Imai, N. Iwasa, H. Iwasaki, T. Kubo, M. Kunibu, M. Kurokawa, Z. Liu, T. Minemura, A. Saito, M. Serata, S. Shimoura, S. Takeuchi, Y. X. Watanabe, K. Yamada, Y. Yanagisawa, K. Yogo, A. Yoshida, and M. Ishihara, Phys. Lett. B **499**, 233 (2001).
[24] D. Guillemaud-Mueller, Eur. Phys. J. A **13**, 63 (2002).
[25] H. Iwasaki, T. Motobayashi, H. Sakurai, K. Yoneda, T. Gomi, N. Aoi, N. Fukuda, Zs. Fulop, U. Futakami, Z. Gacsi, Y. Higurashi, N. Imai, N. Iwasa, T. Kubo, M. Kunibu, M. Kurokawa, Z. Liu, T. Minemura, A. Saito, M. Serata, S. Shimoura, S. Takeuchi, Y. X. Watanabe, K. Yamada, Y. Yanagisawa, and M. Ishihara, Phys. Lett. B **522**, 227 (2001).
[26] M. Yamagami, E. Khan, and Nguyen Van Giai (unpublished).
[27] E. Khan, N. Sandulescu, M. Grasso, and Nguyen Van Giai, Phys. Rev. C **66**, 024309 (2002).
[28] G. F. Bertsch and S. F. Tsai, Phys. Rep., Phys. Lett. **18C**, 125 (1975).
[29] I. Hamamoto and H. Sagawa, Phys. Rev. C **60**, 064314 (1999).
[30] S.-O. Bäckman, A. D. Jackson, and J. Speth, Phys. Lett. **56B**, 209 (1975).
[31] B. Gall, P. Bonche, J. Dobaczewski, H. Flocard, and P.-H. Heenen, Z. Phys. A **348**, 183 (1994).
[32] J. Terasaki, P.-H. Heenen, P. Bonche, J. Dobaczewski, and H. Flocard, Nucl. Phys. **A593**, 1 (1995).
[33] M. Yamagami, K. Matsuyanagi, and M. Matsuo, Nucl. Phys. **A693**, 579 (2001).
[34] J. Bartel, P. Quentin, M. Brack, C. Guet, and H.-B. Hakansson, Nucl. Phys. **A386**, 79 (1982).
[35] J. Dobaczewski, H. Flocard, and J. Treiner, Nucl. Phys. **A422**, 103 (1984).
[36] E. Chabanat, P. Bonche, P. Haensel, J. Meyer, and R. Schaeffer, Nucl. Phys. **A635**, 231 (1998); **A643**, 441(E) (1998).
[37] P.-G. Reinhard and H. Flocard, Nucl. Phys. **A584**, 467 (1995).
[38] W. Satula, J. Dobaczewski, and W. Nazarewicz, Phys. Rev. Lett. **81**, 3599 (1998).
[39] M. Matsuo, Nucl. Phys. **A696**, 371 (2001).
[40] I. Hamamoto, S. V. Lukyanov, and X. Z. Zhang, Nucl. Phys. **A683**, 255 (2001).
[41] M. V. Stoitsov, J. Dobaczewski, P. Ring, and S. Pittel, Phys. Rev. C **61**, 034311 (2000).
[42] Z. Ren, Z. Y. Zhu, Y. H. Cai, and G. Xu, Phys. Lett. B **380**, 241 (1996).
[43] G. A. Lalazissis, A. R. Farhan, and M. M. Sharma, Nucl. Phys. **A628**, 221 (1998).
[44] M. Barranco and R. J. Lombard, Phys. Lett. **78B**, 542 (1978).
[45] R. Bengtsson, P. Moller, J. R. Nix, and Jing-ye Zhang, Phys. Scr. **29**, 402 (1984).
[46] M. Yamagami, E. Khan, and Nguyen Van Giai, in *Proceedings of the International Symposium on Frontiers of Collective Motions 2002, University of Aizu, Japan*, edited by H. Sagarva and H. Iwasaki (World Scientific, Singapore, 2003), p. 230.